

M31 Globular Clusters in the HST Archive: II. Structural Parameters¹

Pauline Barmby²

Harvard-Smithsonian Center for Astrophysics, 60 Garden St., Cambridge, MA 02138

`pbarmby@cfa.harvard.edu`

Stephen Holland

Department of Physics, University of Notre Dame, Notre Dame, IN 46556-5670

`sholland@nd.edu`

John P. Huchra

Harvard-Smithsonian Center for Astrophysics, 60 Garden St., Cambridge, MA 02138

`huchra@cfa.harvard.edu`

ABSTRACT

We analyze the structural parameters of the largest-available sample of spatially resolved extragalactic globular clusters. The images of M31 GCs were found in a search of HST archival data, described in a companion paper. We measure the ellipticities and position angles of the clusters and conclude that the ellipticities are consistent with being caused by rotation. We find that most clusters' surface brightness distributions are well-fit by two-dimensional single-mass Michie-King models. A few clusters show possible power-law distributions characteristic of core-collapse, but the spatial resolution is not high enough to make definitive claims. As has been found for other galaxies, the metal-rich clusters are slightly smaller than the metal-poor clusters. There are strong correlations between structural properties of M31 GCs, as for Milky Way clusters, and the two populations are located close to the same 'fundamental plane' in parameter space.

Subject headings: galaxies: individual (M31) – galaxies: star clusters

²Guest User, Canadian Astronomy Data Centre, which is operated by the Herzberg Institute of Astrophysics, National Research Council of Canada.

¹Based on observations made with the NASA/ESA Hubble Space Telescope, obtained from the data archive at Space Telescope Science Institute. STScI is operated by the Association of Universities for Research in Astronomy, Inc. under NASA contract NAS 5-26555.

1. Introduction

Globular clusters’ structures yield important information about their dynamical states and also about the environmental effects of the parent galaxy’s tidal field. The core radii and ellipticities of Galactic globulars are known to vary with position (van den Bergh 1994; White & Shawl 1987), and the mean structural parameters of clusters also vary between galaxies. For example, the LMC’s globular clusters are, on average, much more flattened than those of the Milky Way (van den Bergh 1983). These findings have led to many suggestions and theories about the histories of GCSs and their parent galaxies (e.g., van den Bergh 2000), but these conclusions would be much stronger if structural parameters were accurately measured for clusters in more galaxies.

Globular clusters in Local Group galaxies are particularly valuable for such a comparison. They are distant enough that their integrated properties can be easily derived, but near enough that their individual stars can also be resolved. M31 has the Local Group’s largest globular cluster population, so it is a natural starting place for studies of extragalactic globular clusters. The M31 GCS is known to be similar to the Milky Way’s in numerous ways (e.g., metallicity and spatial distributions; Barmby et al. 2000), but has some important differences as well (chemical composition and possibly age and luminosity distribution: Brodie & Huchra 1991; Barmby, Huchra, & Brodie 2001). While many properties of the M31 globular clusters can be elicited with ground-based imaging and spectroscopy, high spatial resolution data from space-based telescopes such as HST are required to study their spatial structures and stellar populations. The angular sizes of M31 globular clusters are comparable to the sizes of ground-based seeing disks: Schweizer (1979, 1981) and Holland (1998) showed that seeing can lead to substantial errors in the derived structural parameters of galaxies with similar sizes. The first HST measurements (Bendinelli et al. 1993; Fusi Pecci et al. 1994) showed that the ground-based measurements of core and half-light radii were systematically overestimated. To date, post-repair HST measurements of M31 GC parameters (Rich et al. 1996; Grillmair et al. 1996; Holland, Fahlman, & Richer 1997) have included only a total of seven objects.

In a companion paper (Barmby & Huchra 2001, hereafter Paper I), we described the use of HST/WFPC2 images to identify globular clusters and candidates in M31 and thus examine the quality of existing cluster catalogs. That paper contains the details of the HST Archive search and data reduction procedures. In this paper, we derive structural parameters for ‘good’ (category A and B) cluster candidates found in our survey. The objects studied here do not constitute a complete or magnitude-limited sample of globular clusters in M31, and only the clusters which were not specific HST targets can be considered to be a random sample. Some of our new unconfirmed cluster candidates may not be M31 globulars at all. Several of the clusters in our sample — the targets of HST program GO-6699 — may actually belong to M31’s companion galaxy NGC 205. We retain these objects in our sample except when computing correlations between cluster properties and location in the galaxy. We have studied a much larger sample of M31 globular clusters than has been previously available, and this allows us to explore correlations of structural parameters with other properties such as galactocentric distance, and to determine mean structural properties for

comparison with other galaxies.

2. Surface Brightness Distributions

2.1. Color gradients

Aperture photometry in multiple filters can be used to search for radial color gradients in GCs. Since there is no evidence for internal extinction in GCs, radial color variations are thought to indicate variations in the cluster stellar population. Djorgovski et al. (1991a,b) studied color variations in 12 Milky Way globulars over linear scales of 0.04–4 pc and found the core-collapsed clusters to be bluer in the center, either because of an excess of blue straggler stars or a deficit of red giants. The color gradients in the core-collapsed clusters were 0.1–0.3 mag per decade in radius; non-collapsed clusters did not show any color gradients. The measurement of color gradients in globular clusters is subject to a number of systematic uncertainties, including flat-fielding, contamination from background objects and from M31, absolute centering, centering differences between filters, and stellar population sampling. Using color gradients to detect core-collapsed clusters in M31 is an attractive idea, since it might require lower spatial resolution than a detection from the surface brightness profile. Because of the effects listed above, we believe that such a detection would require a much more detailed study than is presented here, including photometry of individual stars and a careful treatment of incompleteness. This examination of integrated color profiles is intended to serve as a preview for a more detailed study.

The aperture photometry described in Paper I was used to measure the color profiles. The color in each annulus was computed as

$$C_i = C_0 - 2.5 \log \left(\frac{f_1(r_i) - f_1(r_{i-1})}{f_2(r_i) - f_2(r_{i-1})} \right) \quad (1)$$

where f_1 and f_2 refer to the fluxes measured in the two different filters. All of the color profiles are referenced to the color in the central aperture C_0 . The color profiles had a wide variety of appearances: we show a sample in Figure 1. As expected, the profile appearance was much more ‘ragged’ for shorter exposure times and bluer filters, which yielded many fewer counts and hence much more uncertain fluxes. Bright, rich clusters tended to have smooth color profiles, while the looser clusters had much more variable profiles, as might be expected from population sampling statistics. To illustrate this, we used the method of Renzini (1998) to estimate the projected number density of red giants inside the clusters’ half-light radii in the absence of population gradients. The values ranged from ~ 200 stars arcsec $^{-2}$ for typical bright clusters to ~ 2 stars arcsec $^{-2}$ for the faintest and loosest clusters.

We checked the profiles for significant color gradients using a Monte Carlo technique, resampling each profile 10^4 times by bootstrapping and computing the weighted least-squares fit to a straight line. If the absolute value of the computed slope for the real dataset was in the 95th

percentile of the distribution of the absolute value of the slope for the bootstrapped datasets, we considered it to be significant. There were a total of 18 significant color gradients, with two objects having gradients in more than one color. The gradients are comparable in size to those obtained by Djorgovski et al. (1991a) for Milky Way globulars. Strangely, the two gradients for 109–170 (see Figure 1b) are in opposite directions: the center of the cluster is redder in F450–F606W and bluer in F555W–F814W. The F450W/F606W and F555W/F814W image pairs were obtained at different times, so the different color gradients might be due to a bright variable star in the cluster or to cosmic ray contamination in one image pair. $H\alpha$ emission could also have contaminated the F606W image. Overall, two thirds of the slopes are positive (the center is bluer, as found for Milky Way core-collapse objects) and one third are negative (as might be expected for objects which are actually background galaxies).

There is some previous work on M31 GC color gradients: Holland et al. (1997) found gradients of -0.028 and -0.090 magnitudes arcsec^{-1} for 240–302 and 379–312, respectively. We find no significant gradient for 240–302 (shown in Figure 1), and a smaller gradient, -0.02 mag arcsec^{-1} , for 379–312. Since we use the same observational data as Holland et al. (1997), the discrepancy may be related to the fitting or background subtraction methods. Grillmair et al. (1996) found no significant color gradients for 006–058, 045–108, 343–105, and 358–319; we concur with their results for the first three clusters and find a small gradient (0.02 mag arcsec^{-1}) for 358–319. The small sizes of the well-determined gradients and the many possible systematics suggests that definitive measurements of population gradients in M31 GC using integrated colors requires a more detailed study, and possibly better data, than are available here.

2.2. Shape and Structural Parameters

To measure clusters’ shapes, we used the IRAF task ELLIPSE to fit elliptical isophotes to the background-subtracted images. Isophotes were fit over a range of semi-major axes spaced logarithmically from $0.2''$ to $5.0''$ or the largest measurable size. ELLIPSE could not be made to converge for 9 sparse clusters. This was not unexpected, since the algorithm was designed for galaxies and expects the surface brightness distribution to be smooth and monotonically decreasing outward. We were able to estimate shape parameters for about a third of these objects by resampling the images to a resolution of $0.2''/\text{pixel}$ and running ELLIPSE on the ‘blurred’ images. This procedure did not work for the remainder of the images, and objects with no shape measurements are noted in Table 1 with a default zero ellipticity and position angle.

Figure 2 shows some sample ellipticity ($\epsilon = 1 - b/a$) and position angle profiles, plotted as a function of the effective radius ($R_e = \sqrt{ab} = a\sqrt{1 - \epsilon}$) to allow for simple comparison of objects with different ellipticities. In most cases, the ellipticities and position angles measured on images in different filters track well together, as we would expect. The measured position angles are occasionally wildly varying, often when the ellipticities are close to zero. This is likely an artifact of the ELLIPSE algorithm, which diverges as the ellipticity approaches zero (Jedrzejewski 1987).

For these objects, we report ellipticities and position angles of zero in Table 1. We averaged the ELLIPSE output over the isophotal semi-major axes to determine the overall ellipticity, position angle, and central position for each of the cluster images. We further averaged over the different filters to compute the ellipticities and position angles given in Table 1.

Our measured ellipticities generally agree quite well with those of Staneva, Spassova, & Golev (1996), the most comprehensive published dataset. The median difference between two sets of measurements is 0.024 ± 0.009 . Our measured position angles do not agree particularly well with those measured by Staneva et al. (1996), although the agreement is better for more elliptical objects, for which the position angle can be more precisely determined. There are numerous possible sources of systematic differences in ellipticity and position angle measurements, including isophote centering, size of the semi-major axis steps, the adopted algorithm, the image bandpass, and seeing and guiding errors (which could have significant effects on the ground-based results). A comparison of position angles measured by Staneva et al. (1996) and Lupton (1989) shows that the measurements in these two works also agree rather poorly. As most of the ellipticities are small, precise measurement of position angles is not critical to our surface brightness modeling and the discrepancies are not a serious concern. The median ellipticity of the M31 clusters is 0.11 ± 0.01 , in reasonably good agreement with the measurements of Staneva et al. (1996) (0.09 ± 0.04) and Lupton (1989) (0.08 ± 0.02). The clusters’ position angles show no tendency to align with either the major or minor axes of M31, or with the local direction toward the center of the galaxy. This indicates that tidal forces are not responsible for the M31 GCs’ ellipticities; White & Shawl (1987) came to the same conclusion for the Milky Way clusters.

We next fit single-mass, elliptical Michie-King (Michie 1963; King 1966) (hereafter simply ‘King models’) to the cluster images. As usual, we parameterize the models with the scale radius³ r_0 , the concentration $c = \log(r_t/r_0)$ (r_t , the tidal radius, is where the projected cluster density drops to zero), and $\mu(0)$, the central surface brightness. We used the program KM2DFIT written by S. Holland (described in Holland, Côté, & Hesser 1999) to do the model fits. Although KM2DFIT can also fit for the ellipticity, position angle and central position, increasing the number of parameters greatly increases the execution time so we used the ELLIPSE values for these parameters instead. For most objects, we fit the models to the clusters over sub-images $12.8''$ in size. Some objects near the edges of the WFPC2 chips had to be fit in smaller sub-images, and a few were so close to the chip edge that they could not be fit at all (these are marked in Table 1).

The models were convolved with the appropriate WFPC2 PSF before being compared to the data; this greatly increased the execution time but should result in more accurate parameters for the smaller objects. We tried fitting models without PSF convolution, and found that the resulting scale radii were systematically larger (by $0.076 \pm 0.013'' = 0.3$ pc) and the concentrations smaller (by 0.09 ± 0.02) than for the convolved models. This shows that the size of the PSF cannot be

³Binney & Merrifield (1998) point out that r_0 is usually called the core radius and denoted r_c , but r_0 as defined by King (1966) is approximately the same as r_c (the half-intensity radius) only for concentrated clusters.

ignored, even with HST resolution. To check the effect of pixel size (i.e., whether a cluster was imaged on the PC or one of the WFC chips), we selected PC images of 10 clusters with a range of structural parameters, rebinned them to the lower WFC resolution, and re-fit models to the rebinned images. The differences between the PC and WFC models were small: median offsets were $0.01 \pm 0.04'' = 0.04 \pm 0.16$ pc in r_0 , and 0.04 ± 0.04 in c .

Measurement of the same object imaged in more than one filter generally gave quite similar results; the median absolute differences in recovered parameters were 0.13 ± 0.04 in c and $0.04 \pm 0.02'' = 0.15 \pm 0.08$ pc in r_0 . These values provide reasonable estimates of the systematic uncertainties in c and r_0 . The tidal radii are more uncertain since they depends on both of these parameters: error propagation for median values of c and r_0 yields an estimate of $\Delta r_t \approx 2''$. The situation was similar for objects imaged in more than two filters, although fits in the F300W and F336W were often discrepant from others. The poorer signal-to-noise in these filters and/or a different spatial distribution of the horizontal-branch stars (which emit most of the UV light) are the likely causes of the discrepancy. Table 1 gives average King model parameters r_0 , c and r_t for each cluster, and the central surface brightness in the V-band (or another filter if V was unavailable). The central surface brightness is determined by transforming the model central intensity in counts per pixel to magnitudes per square arcsecond using the same calibration as in Paper I.

It would be useful to know if there were any systematic effect of exposure time on the model-fitting results. One could imagine that longer exposure times t relative to a cluster’s integrated magnitude might allow better detection of faint stars at the edge of the cluster, and hence yield larger r_t and c values. Unfortunately it is not possible to directly examine the relationship between the number of photons in a cluster’s image $N_p \propto t \times 10^{-0.4V}$ and the derived King-model parameters. N_p is strongly related to cluster integrated magnitude — brighter clusters emit more flux *and*, in our HST sample, generally have larger t — which is known to correlate with c for Milky Way clusters (we will show below that the same correlation holds for M31 clusters). Instead, we sorted the clusters into 18 pairs with nearly the same V magnitudes ($\Delta V < 0.1$ mag) and values of N_p differing by more than a factor of 1.5. The clusters with larger N_p had larger values of r_0 in 11 of 18 cases, and larger values of c in 10 of 18 cases. We conclude that there does not appear to be a systematic difference in the measured cluster parameters with N_p .

In Figure 3, we compare our measurements of structural parameters with previous HST and ground-based measurements. The agreement is good for r_0 and r_h and rather poor for $\mu_V(0)$ and r_t . The poor agreement for the central surface brightness is likely due to cluster flux being smeared out by the PSF in the previous measurements. Fusi Pecci et al. (1994) used deconvolved (pre-COSTAR) Faint Object Camera images, and Davoust & Prugniel (1990) used ground-based images with PSF deconvolution. The poor agreement in r_t may be attributable to the ground-based measurements by Cohen & Freeman (1991), which are highly uncertain for individual clusters. The large bright cluster 000–001 (also known as G1 or Mayall II) has been previously studied by Rich et al. (1996) and Meylan et al. (2001). The structural parameters for all three works are given in Table 2; all agree fairly well on the values of r_0 and $\mu_V(0)$ but disagree by about a factor of 5 on r_h and r_t .

Different methods used by the different groups may be the causes of the disagreement. The r_t value of Rich et al. (1996) is based on a detection of the tidal cutoff in the surface brightness profile, while ours is based on the c measured from the overall shape of the profile. Because most of the weight in our fit comes from the bright inner regions of the cluster, small variations from a pure single-mass King profile will bias our r_t away from the true value. Meylan et al. (2001) fit multi-mass (instead of single-mass) King models to the one-dimensional surface brightness profile, although they do not correct for the PSF. Gunn & Griffin (1979) suggest that it is quite reasonable for r_t in a multi-mass model to differ by a factor of 2 from that in a single-mass model. G1 is an interesting cluster for many reasons, and a more detailed investigation its surface brightness distribution than is carried out here could be useful.

A final step in checking the modeling results is the examination the differences between modeled and measured surface brightness profiles. Figure 4 shows a sample of these residuals, which are generally less than 10%. The figure also demonstrates the different physical sizes of the clusters; the points stop at the radius where ELLIPSE can no longer fit the isophotes because of poor signal-to-noise. An important question to be addressed by examining the profiles is whether there is evidence for systematic departures of the data from the model profiles. Departures at large radii can indicate the presence of extra-tidal stars, while departures at small radii can indicate the presence of the core-collapse phenomenon. Both effects have been claimed in M31 GCs, by Holland et al. (1997), Grillmair et al. (1996), and Fusi Pecci et al. (1994). Examining the profiles, we find evidence that the following clusters appear to have extra-tidal stars: 006–058, 058–119, 110–172, 240–302, 358–219, and 379–312. We are in agreement with the results of Holland et al. (1997) and Grillmair et al. (1996) for all objects except 343–105, which Grillmair et al. find to have extra-tidal stars and we do not. A potential problem with detections of excess flux at large radius is the uncertain effects of background subtraction. We tried to account for this in our model-fitting by allowing the background level to vary even though it should have been set to zero by our subtraction procedure.

Detecting core-collapsed clusters is difficult: even in the Milky Way, detections of core-collapse in GC surface brightness profiles came many years after the phenomenon was first predicted (see, e.g., Djorgovski & King 1984). Core-collapsed globular clusters are distinguished from ‘King-model’ clusters by the fact that their surface brightness profiles are better fit by a power law. To check for core collapse in M31 GCs, we fit power-laws to the ELLIPSE surface brightness profiles and compared the RMS deviation between the power-law model profiles and the data to that between King model profiles and data. As expected, most of the clusters were better fit by King models than by power laws. The profiles of a few objects, mostly those for which the best-fit King models had large values of c , were fit as well as or better than King models by power laws. These may be core-collapsed clusters; we show their profile residuals in Figure 5 and mark them in Table 1. Bendinelli et al. (1993) and Grillmair et al. (1996) both suggested that 343–105 showed signs of core collapse in its profile, while we find that the King model is formally a slightly better fit than the power law for this object. The two previous works deconvolved the observed profile from the PSF before fitting a power law, which may be why they measured a slightly different profile. However,

as Figure 5 shows, there is very little difference between the two models, and we believe it is very difficult to use the existing data to differentiate between the profile of a high-concentration King model with a small scale radius (for 343–105 we measured $r_0 = 0.42$ pc) and a power-law one with existing data.

3. M31 and Milky Way Globular Cluster Comparisons and Correlations

The structural parameters of globular clusters are the result of both their current and past dynamical conditions. It is therefore of interest to compare the measurements of M31 globular clusters to those of clusters in other galaxies, primarily the Milky Way, and to search for correlations among their properties. We used the June 1999 version of the Harris (1996) catalog as our source of Milky Way cluster properties⁴, supplemented by the White & Shawl (1987) data on cluster ellipticities.

3.1. King Model Parameters

M31 and Milky Way globular cluster structural parameters are shown in Figure 6. While the two galaxies’ GCs follow essentially the same trends, the M31 clusters cover a much smaller range of sizes and central surface brightnesses than the Milky Way clusters. The largest scale radius for a Milky Way cluster is 20.2 pc (Pal 14); the largest scale radius we measured for a confirmed M31 GC is 6.1 pc (468–000). Comparing M31 clusters to non-core-collapsed Milky Way clusters with the same range of central surface brightness, we find the median r_0 to be 0.77 pc for the M31 clusters and 1.14 pc for the Milky Way clusters. The difference is almost certainly due to selection effects: most of the targeted HST observations were of bright M31 clusters with high central surface brightness, and larger low-surface-brightness clusters (the ‘Palomar’-type Milky Way clusters are the extreme examples) would have been very difficult to detect in M31. The lowest surface brightness objects we expect to detect in our median exposure have $\mu_V(0) \approx 20$.

Except for the lack of confirmed core-collapsed clusters in M31, discussed in the previous subsection, the range of concentration parameters is similar for the M31 and Milky Way clusters. The median values of c are 1.40 for the non-core-collapsed Milky Way clusters and 1.43 for the M31 clusters. Six of our M31 clusters fall into a region of parameter space where no Milky Way clusters are found: $c \lesssim 1.1$, $r_0 < 1$ pc (these objects are also the outliers in the r_0, r_h plot). The identities of all are questionable: 132–000 had been previously been classified as a star from its spectrum (Barmby et al. 2000), 268–000 is an unconfirmed C-class cluster from Battistini et al. (1987) with few known properties, 000–M91 is an unconfirmed candidate first discovered by Mochejska et al.

⁴Note that the central surface brightness measurements reported in the Harris catalog are not corrected for extinction, although the absolute magnitudes are.

(1998), and the other three objects are new cluster candidates. All are faint and small; several have rather poor fits to the King models. Three are projected very close to the center of M31. Their estimated relaxation times at the half-mass radius range from 2×10^7 to 2.5×10^8 yr. The relaxation times are quite short compared to the Hubble time, and if the objects projected near the center of M31 are truly near the nucleus, they should have been destroyed long ago. We are uncertain about the nature of these objects, and suggest that higher resolution images and/or spectra may be needed to fully understand them. To confirm that the M31 clusters are well-characterized by King models, we performed a principal component analysis with the five structural parameters M_V , $\mu_V(0)$, r_0 , r_h , and c . We find, as did Djorgovski & Meylan (1994) for the Milky Way clusters, that the dimensionality of this dataset is $D = 3$. The three-parameter King model is adequate to describe the surface brightness profiles of M31 globular clusters.

3.2. Galactocentric distance

Figure 7 shows the Milky Way and M31 structural parameters as a function of galactocentric distance R_{gc} . There is no clear correlation of $\mu_V(0)$ with R_{gc} , except for the tendency, mentioned above, for the very low surface brightness Milky Way GCs to be located far from the galaxy center. This is unsurprising, since such clusters would be easily destroyed by dynamical forces nearer to the galaxy center. Also expected from dynamical considerations is that core-collapsed clusters should have smaller average R_{gc} (since the stronger tidal field accelerates the clusters' dynamical evolution); Figure 7 shows that this is true for the Milky Way. Most of the M31 core-collapse candidates are within 2 kpc of the center of M31, and a KS test shows the R_{gc} distributions of the core-collapse candidates and the rest of the sample to be different at the 95% confidence level. There is no significant trend of c with R_{gc} for the *non*-core collapsed clusters in either M31 or the Milky Way. Both r_h and r_0 are correlated with galactocentric distance, which has been noticed before for Milky Way clusters (van den Bergh, Morbey, & Pazder 1991). These authors suggest that, while large clusters with small R_{gc} could have been destroyed, there is no equivalent reason for the lack of small clusters at large R_{gc} , so the correlation is due to physical conditions at the time of cluster formation. The data in Figure 7 suggest that similar conditions affected the formation of the M31 globular clusters.

3.3. Ellipticities

Cluster rotation, rather than tidal forces, is the generally accepted explanation for cluster flattening. A general picture, summarized by Davoust & Prugniel (1990), is that GCs form with some angular momentum and are initially flattened by rotation. As escaping stars carry away angular momentum and mass, clusters rotate more slowly and become rounder. The rotation model makes several predictions. One is that more compact clusters, which evolve more quickly, should be rounder. White & Shawl (1987) found this to be the case for Milky Way clusters. We

plot ellipticity against several other parameters for both sets of clusters in Figure 8. We find no clear relation between c and ϵ for Milky Way clusters, but we do see that low-concentration clusters in M31 are generally more elliptical, as predicted. A second prediction is that clusters with larger velocity dispersions should be rounder because they rotate more slowly, due to conservation of angular momentum in the sum of internal velocity dispersion and rotation (Staneva et al. 1996). These authors find a relation between ϵ and σ_v in M31 clusters in their data, but when we add later velocity dispersion measurements by Djorgovski et al. (1997) to Staneva et al.’s ellipticity data, we see no obvious correlation.

Conflicting claims have been made about correlations of globular cluster ellipticities with other properties. Lupton (1989) claimed that ellipticity was anti-correlated with metallicity for both Milky Way clusters and his sample of 18 M31 clusters; Staneva et al. (1996) and White & Shawl (1987) found no such correlation. Our data in Figure 8 show little correlation (only about half of our M31 clusters have measured metallicities), but if we bin the data in $[\text{Fe}/\text{H}]$ we find that the most metal-poor objects are slightly more elliptical. Davoust & Prugniel (1990) claimed a relation between luminosity and ellipticity for both M31 and Milky Way clusters, with the brightest clusters being the roundest; Staneva et al. (1996) found the same for M31.⁵ Lupton (1989) did not find a luminosity-ellipticity relationship in his sample. Our data again show no clear correlation, but with binned data we do find that the least-luminous clusters tend to be more elliptical. White & Shawl (1987) found that the most elliptical Milky Way clusters were found near the galactic plane but did not claim a correlation of ϵ with R_{gc} ; Staneva et al. (1996) and Lupton (1989) also found no such correlation in their M31 cluster samples. We find a slight trend in the opposite direction: the innermost clusters are slightly less elliptical. Djorgovski & Meylan (1994) found no correlations of Milky Way GC ellipticity with any other properties, and suggest that this may be because of the difficulties in measuring ellipticity: the effect and its measurement errors are of comparable size. Our results suggest that there may be more subtle effects in the M31 globular cluster system which Djorgovski & Meylan did not find in the MW system.

3.4. Metallicities

As noted above, there is some weak evidence for lower-metallicity M31 clusters to be more elliptical. Figure 9 shows that there is essentially no correlation of metallicity with concentration or central surface brightness, but there does appear to be a correlation with size, as measured by r_0 or r_h . This has been noticed before: examining globular cluster systems in many galaxies, both Kundu et al. (1999) and Larsen et al. (2001) found that the metal-rich clusters had slightly smaller average values of r_h . We assigned M31 clusters to metallicity groups based on either spectroscopic

⁵The brightest clusters in each galaxy, ω Cen and G1, are both quite flattened, with $\epsilon \sim 0.2$. There have been suggestions that neither object is a true globular cluster (Hilker & Richtler 2000; Meylan et al. 2001), so their failure to follow this trend may not be meaningful.

metallicities, color-derived metallicities from Barmby et al. (2000), or the HST $V - I$ color (the criterion used by Larsen et al. 2001). Figure 10 shows size distribution for the two groups. The median sizes for the two groups are similar to values found for other galaxies: 2.17 pc for the metal-rich clusters and 2.76 pc for the metal-poor ones. Some of the size difference could be due to R_{gc} : metal-rich clusters are more likely to be near the center of M31, and we have already shown that there is a gradient of r_h with R_{gc} . There is still a size difference between the two metallicity groups for clusters with $R_{gc} > 2$ kpc; however, a KS test does not show the r_h differences to be statistically significant, and the small number of metal-rich clusters (17 in total and only 11 with $R_{gc} > 2$ kpc) makes our conclusions uncertain. The correspondence with the results for the Milky Way and other galaxies is certainly suggestive. The size difference could indicate the different pericenter distances of the clusters’ orbits, as might be expected from their different kinematics.

3.5. Parameter Correlations and the Fundamental Plane

Globular cluster structure is described by four parameters: concentration c , scale radius r_0 , central surface brightness $\mu_V(0)$, and central mass-to-light ratio Υ_0 or velocity dispersion σ_0 . Figure 6 shows that there are strong correlations between the King model parameters of both Milky Way and M31 globular clusters, meaning that clusters do not inhabit the full four-dimensional parameter space. Djorgovski (1995) found a pair of bivariate correlations in Milky Way GC parameters which imply the existence of a ‘globular cluster fundamental plane’. Only about 20 M31 GCs have measurements of mass-to-light ratios (Dubath & Grillmair 1997; Djorgovski et al. 1997), but they appear to fall on the same plane as the Milky Way clusters. Bellazzini (1998) posited the existence of a ‘fundamental straight line’ as expected if GCs represent a family of objects with constant core mass evolving toward core collapse. McLaughlin (2000) examined the Milky Way GC fundamental plane in detail and disputed Bellazzini’s interpretation, pointing out that cluster cores cannot be viewed as dynamically distinct entities since they do not obey the virial theorem.

Any linearly independent combination of the parameters described above is a complete basis for describing GC structure, and McLaughlin (2000) chose the set c , Υ_0 , luminosity L , and binding energy E_b to describe the Milky Way clusters. He showed that the Milky Way clusters’ fundamental plane was described by the equations

$$\Upsilon_{V,0} = 1.45 \pm 0.1 \quad (2)$$

and

$$E_b = AL^\gamma \Rightarrow \log E_b = (39.89 \pm 0.38) + (2.05 \pm 0.08) \log L \quad (3)$$

Although equation 2 can be used in computing E_b for the Milky Way clusters, this does *not* imply an automatic correlation between E_b and L : the two parameters are linearly independent.

Since our HST observations provide no new information about M31 clusters’ mass-to-light ratios, we cannot directly test McLaughlin’s result of a constant Υ_0 for M31 clusters. However,

McLaughlin used the fundamental plane to predict the existence of several ‘monovariate’ correlations which involve only the King model parameters (his equations A14 and A17). These are:

$$\log r_0 = 41.2208 - \log A + 2 \log \Upsilon_0 + (2 - \gamma) \log L - f(c) \quad (4)$$

and

$$\mu_V(0) = 232.466 - 5 \log A + 10 \log \Upsilon_0 + (7.5 - 5\gamma) \log L - g(c) \quad (5)$$

where A and γ are given above, and f and g are ‘nonhomology terms’ (for details, see McLaughlin 2000). We can use these predictions to see whether the M31 clusters’ properties are compatible with the Milky Way fundamental plane.

Figure 11 plots the difference between the fundamental plane predictions and the measured values of r_0 and $\mu_V(0)$ for M31 and Milky Way GCs. Table 3 gives the statistics of the differences between predicted and measured values (core-collapsed Milky Way clusters are not included). The standard errors of the means are similar for the two sets of clusters, which is somewhat surprising, given that we expect the observational errors to be larger for the M31 data. It implies that the two sets of clusters have about the same amount of scatter about the fundamental plane. The mean values are consistent with zero for the Milky Way clusters, but offset from zero for the M31 clusters. This could imply that the M31 clusters have a different mass-to-light ratio Υ_0 and/or $E_b - L$ intercept A from the Milky Way clusters, or that there are systematic errors in our M31 cluster measurements.

We can test this idea by examining the fundamental plane predictions of E_b as a function of L for the M31 clusters. The difference between E_b predicted from L (using equation 3) and the measured value (computed from McLaughlin’s equation 5c) also has a term of the form $a = 2 \log \Upsilon_0 - \log A$, but with the opposite sign to the r_0 and $\mu_V(0)$ differences. Figure 12 shows the difference between the fundamental plane predictions of $E_b(L)$ and the measured values for M31 and Milky Way GCs. Again the Milky Way clusters’ mean difference is consistent with zero. In this case the M31 clusters have a slightly larger scatter than the Milky Way clusters, as well as an offset. $\Delta \log E_b$ has the same sign as Δr_0 and $\Delta \mu_V(0)$, which means that a different value of a for the M31 clusters cannot simultaneously account for all three offsets.

Can the differences between fundamental plane predictions and M31 GC observations be explained by a combination of true differences between the M31 and Milky Way GC fundamental planes and systematic errors in the observations? Yes. Increasing our measured M31 $\log(r_0)$ values by 0.12 and decreasing a by 0.09, while leaving $\mu_V(0)$ unchanged, resulted in all Δ values consistent with zero. Subtracting 0.57 mag from our measured M31 $\mu_V(0)$ values and decreasing a by 0.20, while leaving r_0 unchanged, gave the same result. The dependence of the Δ values on c (through the nonhomology terms $f(c)$ and $g(c)$ above and $\mathcal{E}(c)$ in E_b) is not as straightforward as that on $\log(r_0)$ and $\mu_V(0)$, but experiment showed that increasing the measured values of c for M31 clusters by 0.25 (with no changes in r_0 or a) resulted in Δ values consistent with zero. Other combinations of parameter changes might also result in a better fit to the fundamental plane, but we concentrate here on the simplest ones.

The systematic changes which improve the M31 clusters’ fit to the Milky Way GC fundamental plane also result in a slightly better match with the Milky Way clusters in Figure 6. This is not surprising, since the correlations shown there are due to the existence of the fundamental plane. But are the changes reasonable? A change in a of 0.09, if interpreted as due to the M31 clusters’ mass-to-light ratio, implies $\Upsilon_{0,\text{M31}} = 1.3$, well within the measured values for M31 clusters. Increasing the measured r_0 by 30% ($\Delta \log(r_0) = +0.12$) would worsen the agreement of our measurements with those by other groups, although it would make the median r_0 for M31 clusters closer to that for Milky Way clusters. A systematic error in r_0 would seem more likely to result in our measured values being too large (because of the limited spatial resolution) rather than too small. Subtracting 0.56 from our measured $\mu_V(0)$ marginally improves the agreement with other groups, and it is plausible that the limited spatial resolution could have resulted in our measuring central intensities which were 60% of the true value. Increasing c by 0.25 (and thereby increasing r_t by $10^{0.25}$) marginally worsens agreement of r_t with other values, but also seems a plausible effect of limited spatial resolution.

More information is needed to distinguish between the various possible reasons for the offset between fundamental plane predictions and M31 cluster observations. The small scatter of the mean M31 offsets implies that the M31 clusters may well have a constant mass-to-light ratio, but additional measurements would be very useful to confirm this and to determine the value of Υ_0 . Additional measurements of King model parameters, both from the existing HST data and from future data, will help to clarify whether there are systematic errors in our method. Even with the offsets, it is clear that M31 and Milky Way clusters have a limited and very similar range of properties, controlled by strong correlations. If additional galaxies’ GCs have similar fundamental planes, this will strengthen the case for a ‘universal’ GC formation mechanism, in which GC properties are controlled by very few parameters (possibly the initial protocluster gas mass: McLaughlin 2000; Bellazzini 1998).

4. Summary

We use HST images of M31 globular clusters to measure the clusters’ sizes, shapes, and best-fit King model parameters. Cluster departures from sphericity are consistent with being caused by rotation, although there are also indications of relations between ellipticity and luminosity and metallicity. We find a slight difference between the half-light radii of metal-rich and metal-poor clusters, consistent with previous results on clusters in other galaxies. The M31 clusters are well-described by the three-parameter family of King models. They have approximately the same range of parameter values as the Milky Way clusters, except that there are few faint, low-concentration clusters in our M31 sample due to observational selection effects. The scatter about the fundamental plane relations is very similar for Milky Way and M31 clusters, although the M31 clusters are offset from the Milky Way cluster relations. This effect may be due to an intrinsic difference in the two galaxies’ clusters’ fundamental planes or to systematic errors in our measurements:

further information is needed. The overall similarity of the two fundamental planes implies that the formation and evolution of GCs must have been very similar in the two galaxies.

We thank J. Grindlay, G. Harris, W. Harris and S. Zepf for helpful discussions, and K. Stanek and R. Di Stefano for critically reading the manuscript. We also thank the referee, whose report was helpful in clarifying several issues.

REFERENCES

- Barmby, P. & Huchra, J. P. 2001, *AJ*, 122, 2458
- Barmby, P., Huchra, J. P., & Brodie, J. P. 2001, *AJ*, 121, 1482
- Barmby, P., Huchra, J. P., Brodie, J. P., Forbes, D. A., Schroder, L. L., & Grillmair, C. J. 2000, *AJ*, 119, 727
- Battistini, P. L., Bònoli, F., Braccisi, A., Federici, L., Fusi Pecci, F., Marano, B., & Börngren, F. 1987, *A&AS*, 67, 447
- Bellazzini, M. 1998, *NewA*, 3, 219
- Bendinelli, O., Cacciari, C., Djorgovski, S., Federici, L., Ferraro, F. R., Fusi Pecci, F., Parmeggiani, G., Weir, N., & Zavatti, F. 1993, *ApJ*, 409, L17
- Binney, J. & Merrifield, M. 1998, *Galactic Astronomy* (Princeton, NJ: Princeton University Press)
- Brodie, J. P. & Huchra, J. P. 1991, *ApJ*, 379, 157
- Cohen, J. G. & Freeman, K. C. 1991, *AJ*, 101, 483
- Davoust, E. & Prugniel, P. 1990, *A&A*, 230, 67
- Djorgovski, S. 1995, *ApJ*, 438, L29
- Djorgovski, S. & King, I. R. 1984, *ApJ*, 277, L49
- Djorgovski, S. & Meylan, G. 1994, *AJ*, 108, 1292
- Djorgovski, S., Piotto, G., & Mallen-Ornelas, G. 1991a, in *ASP Conf. Ser. 13: The Formation and Evolution of Star Clusters*, ed. K. Janes (San Francisco: ASP), 262–264
- Djorgovski, S., Piotto, G., Phinney, E. S., & Chernoff, D. F. 1991b, *ApJ*, 372, L41
- Djorgovski, S. G., Gal, R. R., McCarthy, J. K., Cohen, J. G., de Carvalho, R. R., Meylan, G., Bendinelli, O., & Parmeggiani, G. 1997, *ApJ*, 474, L19

- Dubath, P. & Grillmair, C. J. 1997, *A&A*, 321, 379
- Fusi Pecci, F., Battistini, P., Bendinelli, O., Bònoli, F., Cacciari, C., Djorgovski, S., Federici, L., Ferraro, F. R., Parmeggiani, G., Weir, N., & Zavatti, F. 1994, *A&A*, 284, 349
- Grillmair, C. J., Ajhar, E. A., Faber, S. M., Baum, W. A., Holtzman, J. A., Lauer, T. R., Lynds, C. R. C., & O’Neil, E. J. 1996, *AJ*, 111, 2293
- Gunn, J. E. & Griffin, R. F. 1979, *AJ*, 84, 752
- Harris, W. H. 1996, *AJ*, 112, 1487
- Hilker, M. & Richtler, T. 2000, *A&A*, 362, 895
- Holland, S. 1998, PhD thesis, University of British Columbia
- Holland, S., Côté, P., & Hesser, J. E. 1999, *A&A*, 348, 418
- Holland, S., Fahlman, G. G., & Richer, H. B. 1997, *AJ*, 114, 1488
- Jedrzejewski, R. 1987, *MNRAS*, 226, 1747
- King, I. R. 1966, *AJ*, 71, 64
- Kundu, A., Whitmore, B. C., Sparks, W. B., Macchetto, F. D., Zepf, S. E., & Ashman, K. M. 1999, *ApJ*, 513, 733
- Larsen, S. S., Brodie, J. P., Huchra, J. P., Forbes, D. A., & Grillmair, C. J. 2001, *AJ*, 121, 2974
- Lupton, R. H. 1989, *AJ*, 97, 1350
- McLaughlin, D. E. 2000, *ApJ*, 539, 618
- Meylan, G., Sarajedini, A., Jablonka, P., Djorgovski, S. G., Bridges, T. J., & Rich, R. M. 2001, *AJ*, 112, 830
- Michie, R. W. 1963, *MNRAS*, 125, 127
- Mochejska, B. J., Kaluzny, J., Krockenberger, M., Sasselov, D. D., & Stanek, K. Z. 1998, *Acta Astronomica*, 48, 455
- Renzini, A. 1998, *AJ*, 115, 2459
- Rich, R. M., Mighell, K. J., Freedman, W. L., & Neill, J. D. 1996, *AJ*, 111, 768
- Schweizer, F. 1979, *ApJ*, 233, 23
- Schweizer, F. 1981, *AJ*, 86, 662
- Staneva, A., Spassova, N., & Golev, V. 1996, *A&AS*, 116, 447

- van den Bergh, S. 1983, PASP, 95, 839
- van den Bergh, S. 1994, AJ, 108, 2145
- van den Bergh, S. 2000, PASP, 112, 932
- van den Bergh, S., Morbey, C., & Pazder, J. 1991, ApJ, 375, 594
- White, R. E. & Shawl, S. J. 1987, ApJ, 317, 246

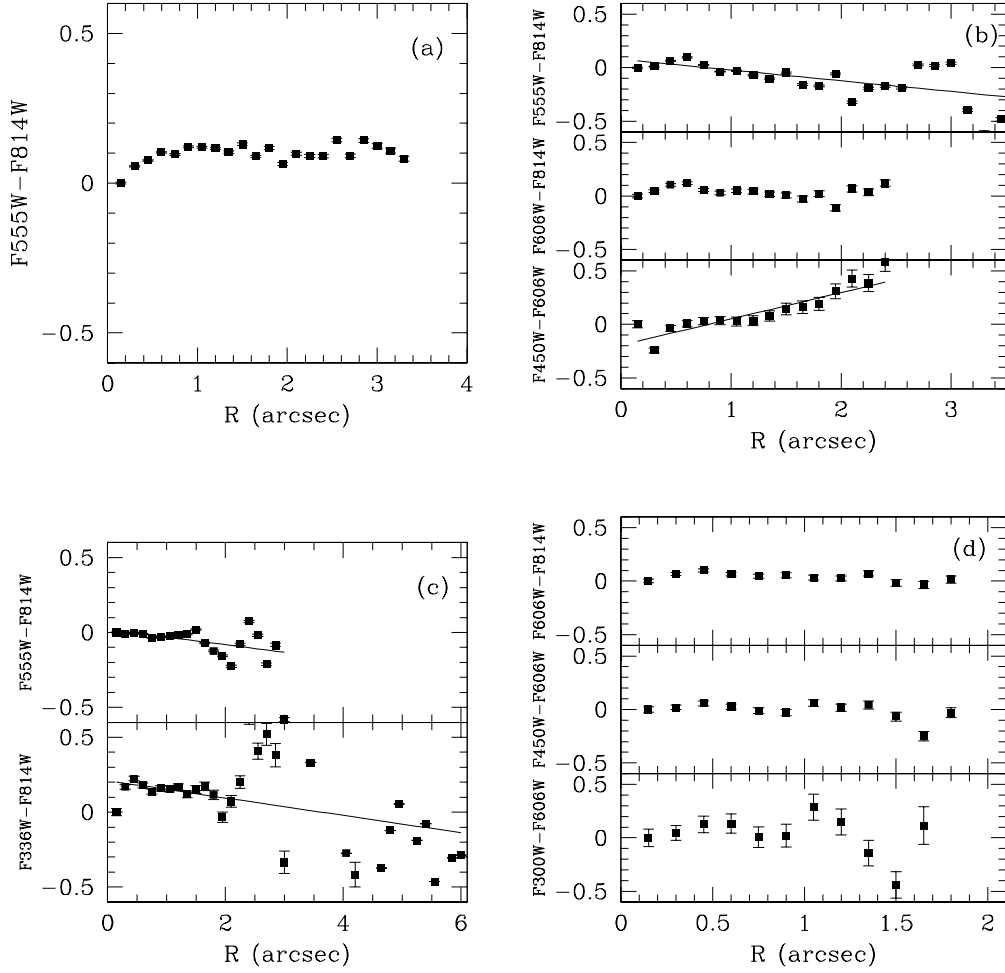


Fig. 1.— Sample color profiles of M31 globular clusters: (a) 240–302 (b) 109–170 (c) 127–185 (d) 076–138. The colors plotted are relative to the color measured in the central aperture. Note that the horizontal axis scales are not identical. Solid lines are the least-squares fits to the color profiles of clusters with gradients.

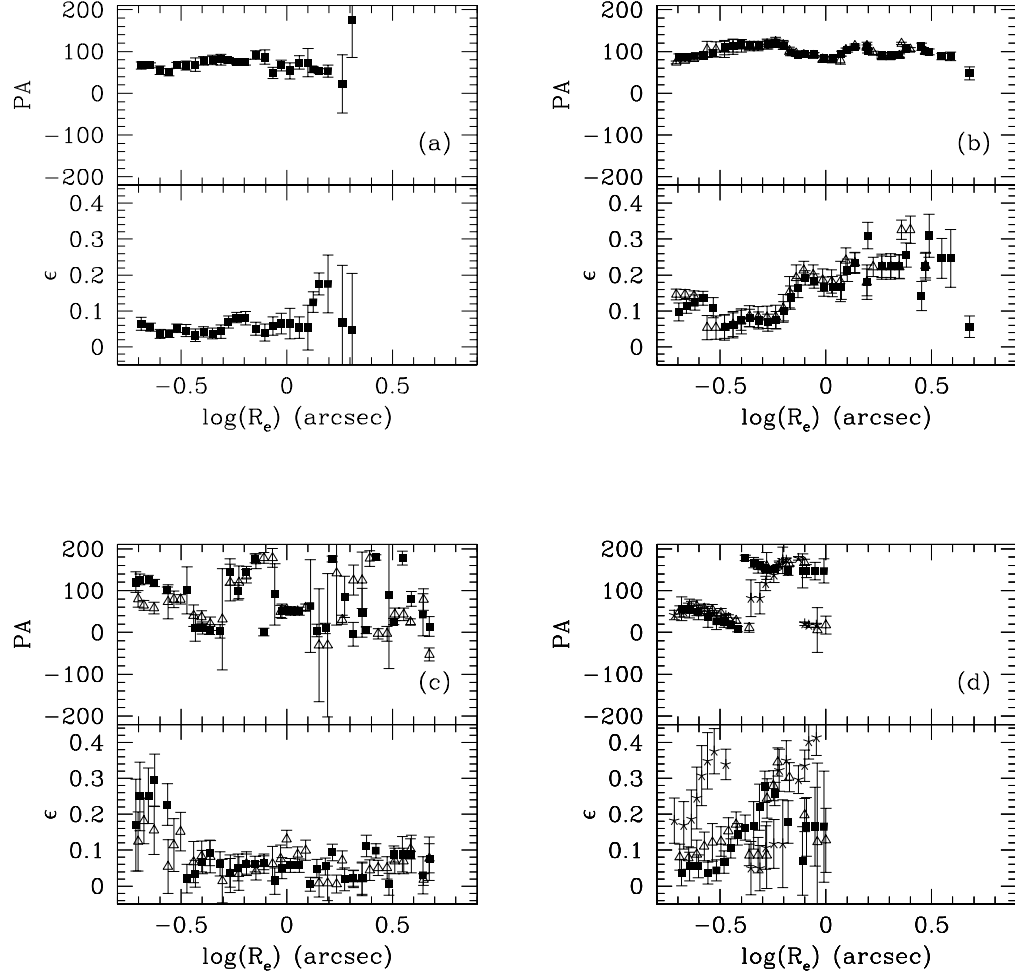


Fig. 2.— Sample ellipticity and position angle profiles for M31 GCs: (a) 153–000 (F300W) (b) 240–302 (F555W, F814W) (c) 338–076 (F555W, F814W) (d) NB39 (F300W, F555W, F814W)

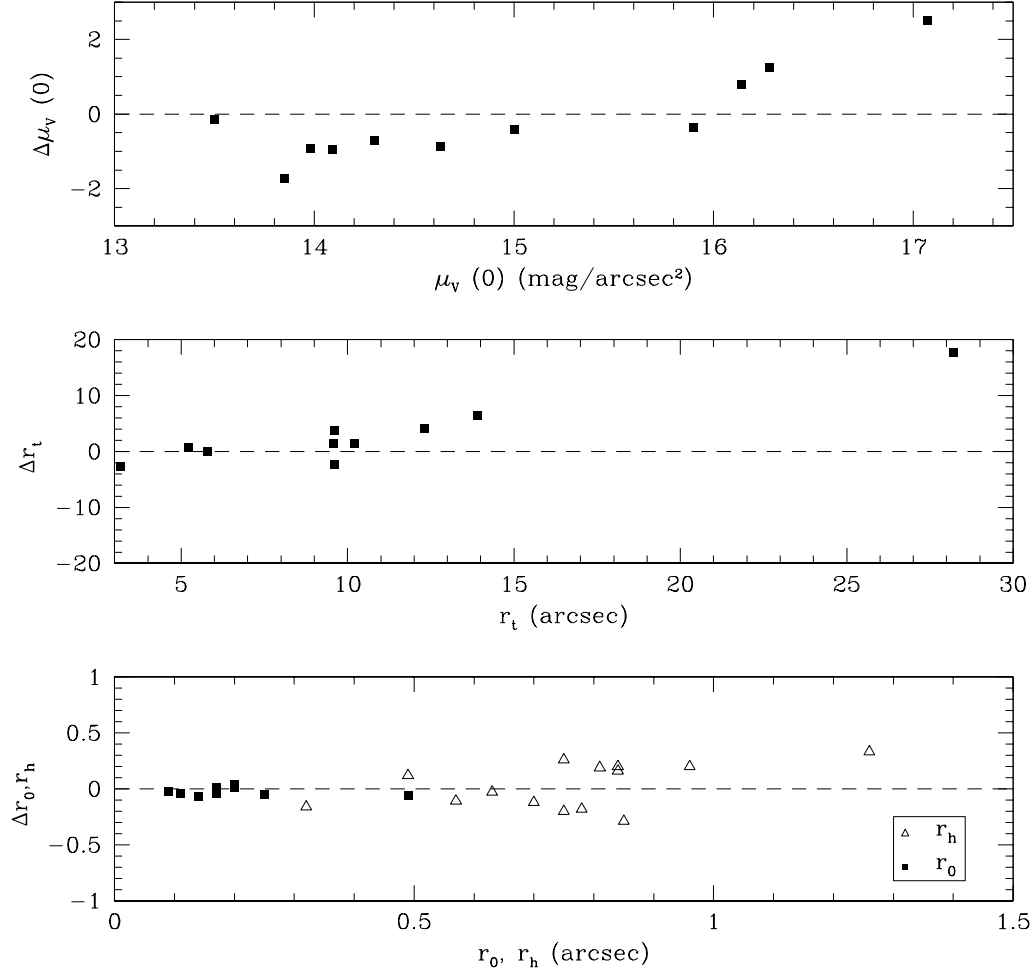


Fig. 3.— Comparison of our measurements of structural parameters with those of previous authors. The horizontal axis is the published measurement; vertical axis is (published – our) measurements.

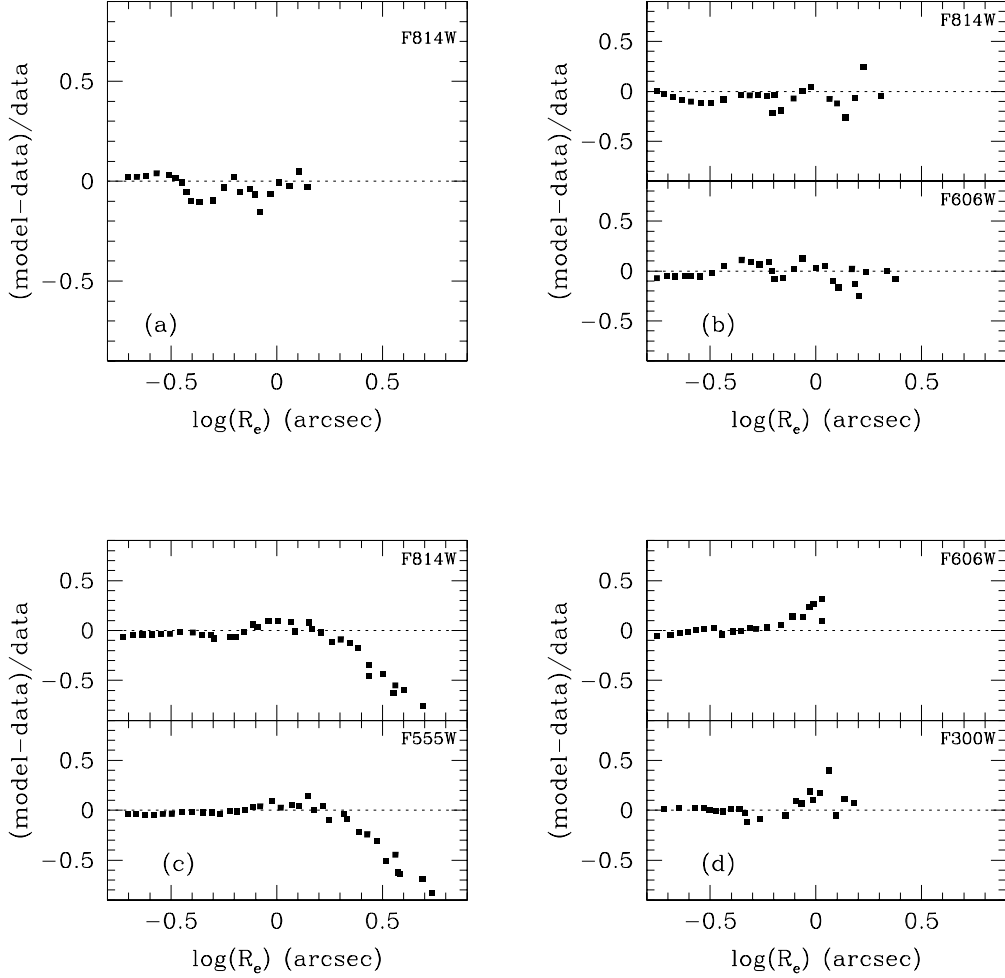


Fig. 4.— Difference between modeled and measured surface brightness profiles for a sample of M31 GCs: (a) 020D-089 (b) 160-214 (c) 006-058 (d) 374-306. 006-058 may have extra-tidal stars.

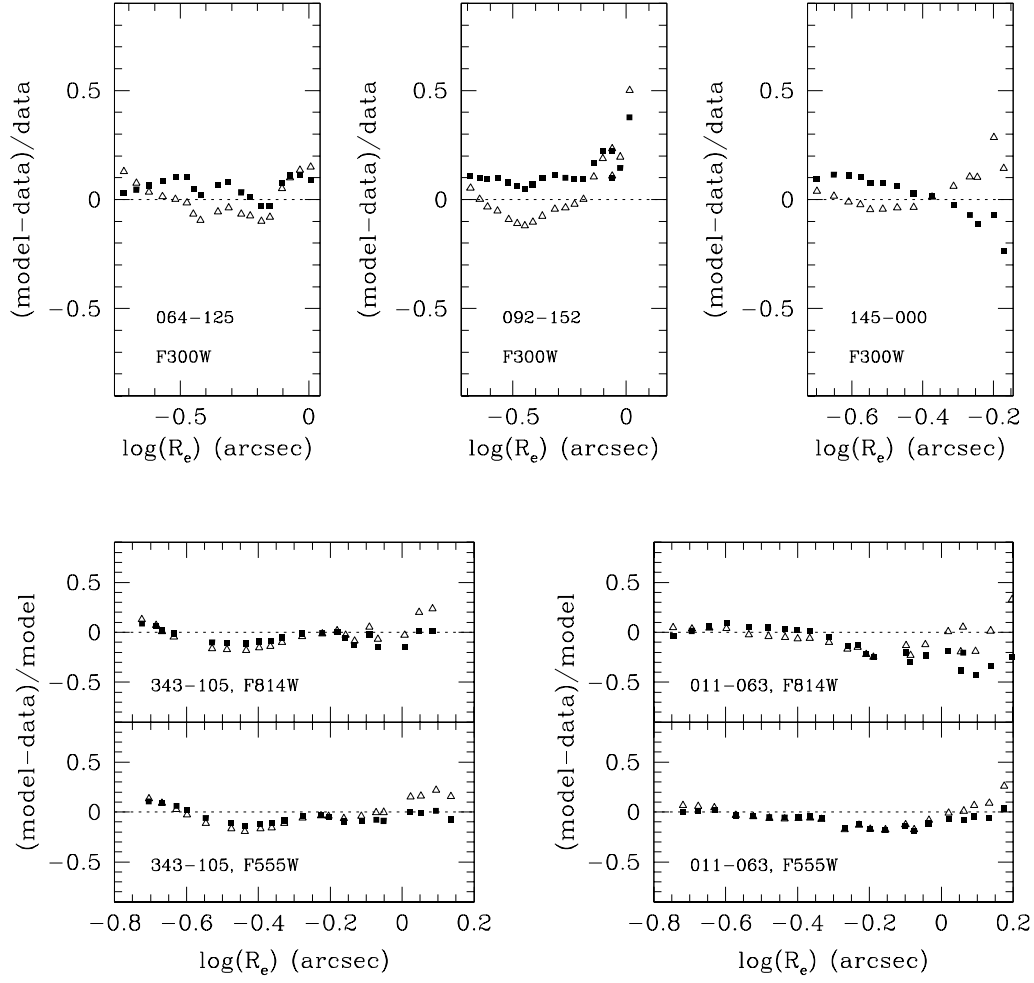


Fig. 5.— Difference between modeled and measured surface brightness profiles for possible core-collapsed M31 GCs. Solid squares are King models – data; open triangles are power-law surface brightness profiles – data.

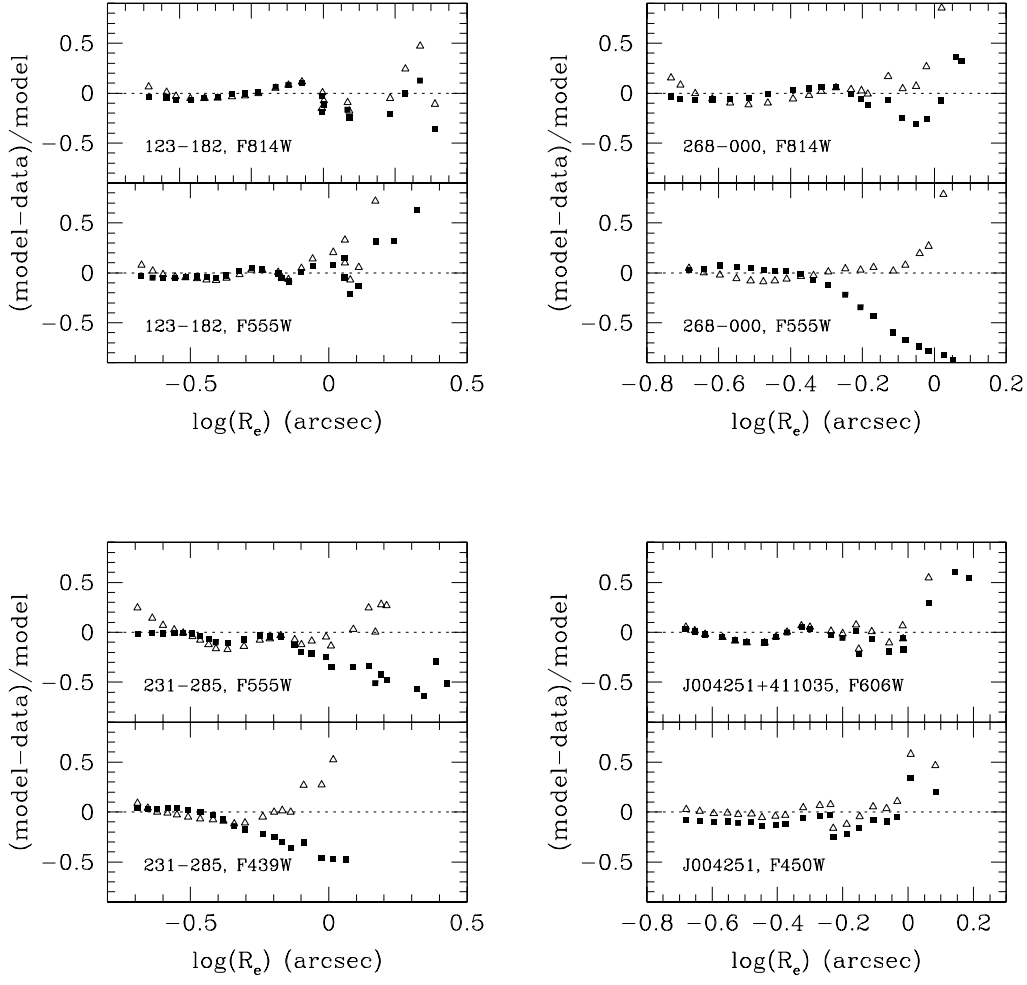


Fig. 5.— Continued.

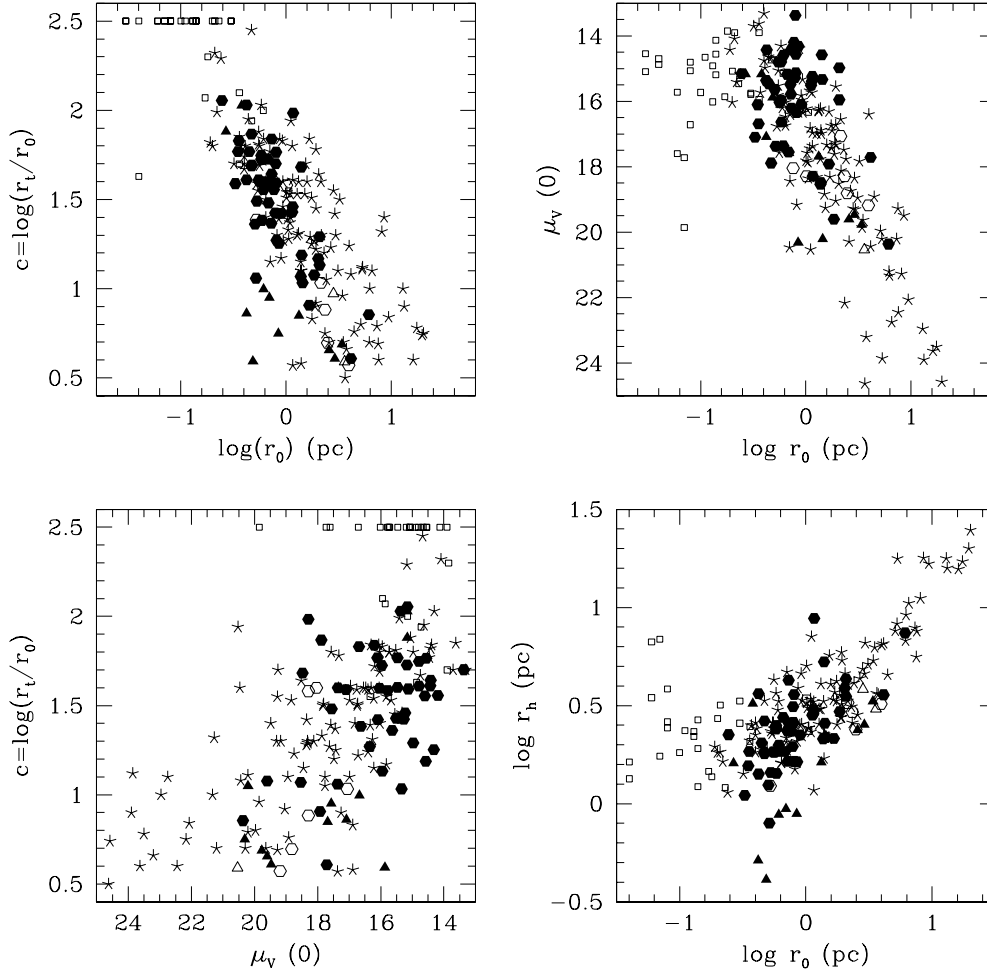


Fig. 6.— King model structural parameters for M31 and MW GCs. Symbols as in Figure 8.

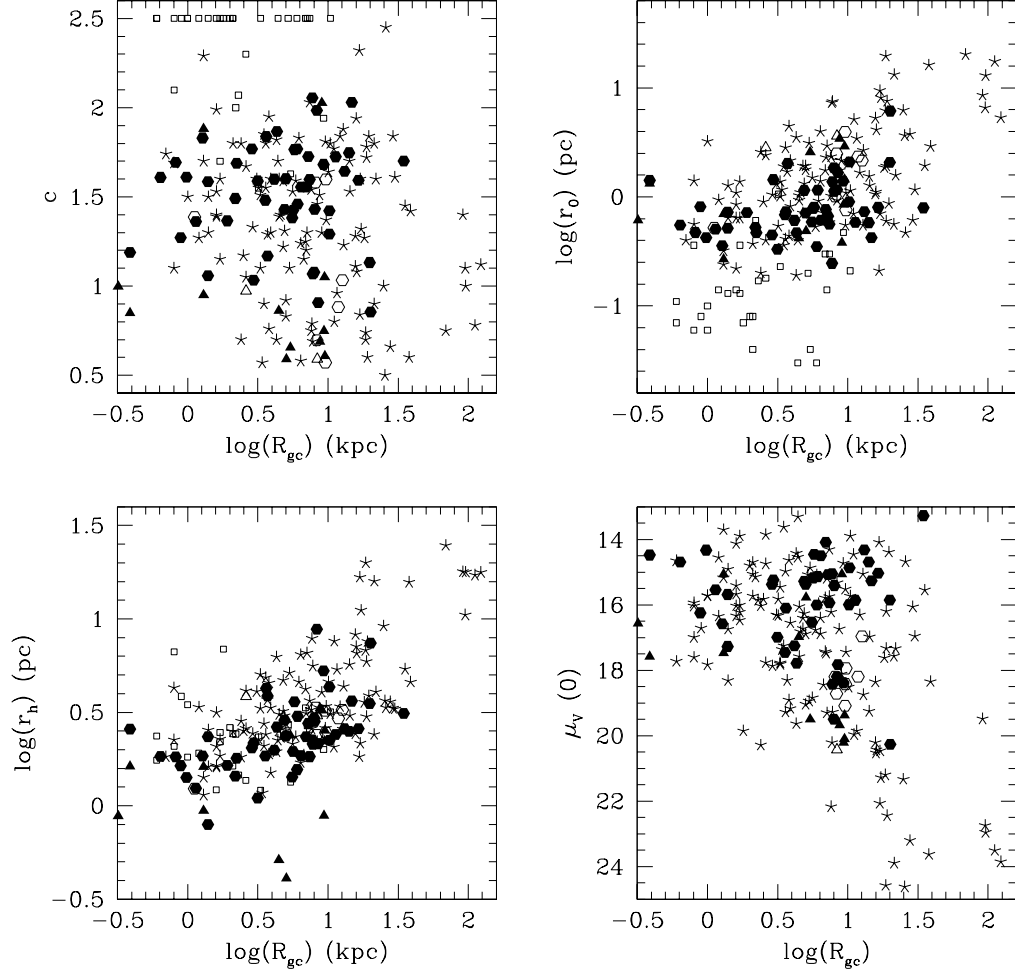


Fig. 7.— Structural parameters of M31 and Milky Way globular clusters as a function of galactocentric distance (true three-dimensional distance for Milky Way clusters and projected distance on the sky for M31 clusters). Symbols as in Figure 8.

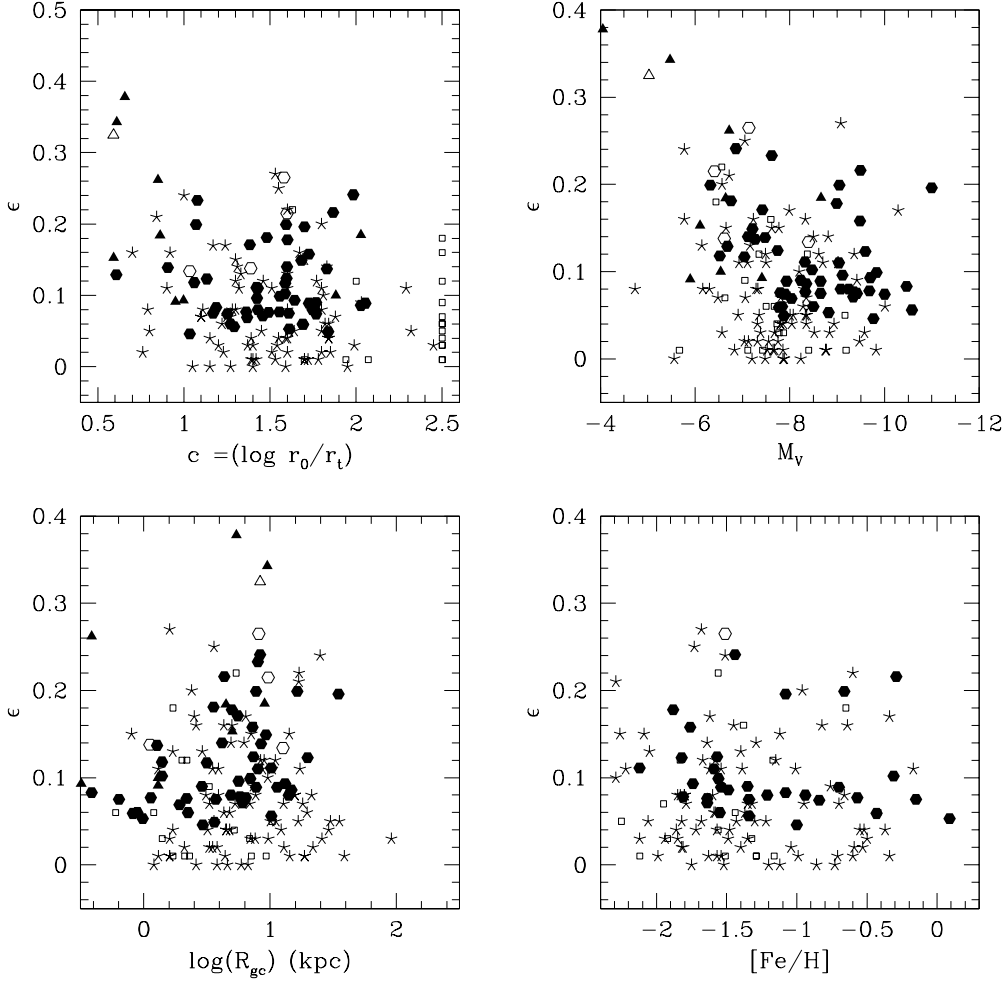


Fig. 8.— Ellipticity versus other properties of M31 and Milky Way globular clusters. Hexagons are previously-known M31 globulars and triangles are new objects. Filled symbols are likely globular clusters; outlined symbols are blue clusters which may not be old GCs. Stars are non-core-collapsed Milky Way GCs; small squares are core-collapsed Milky Way GCs (for which c is set arbitrarily to 2.5).

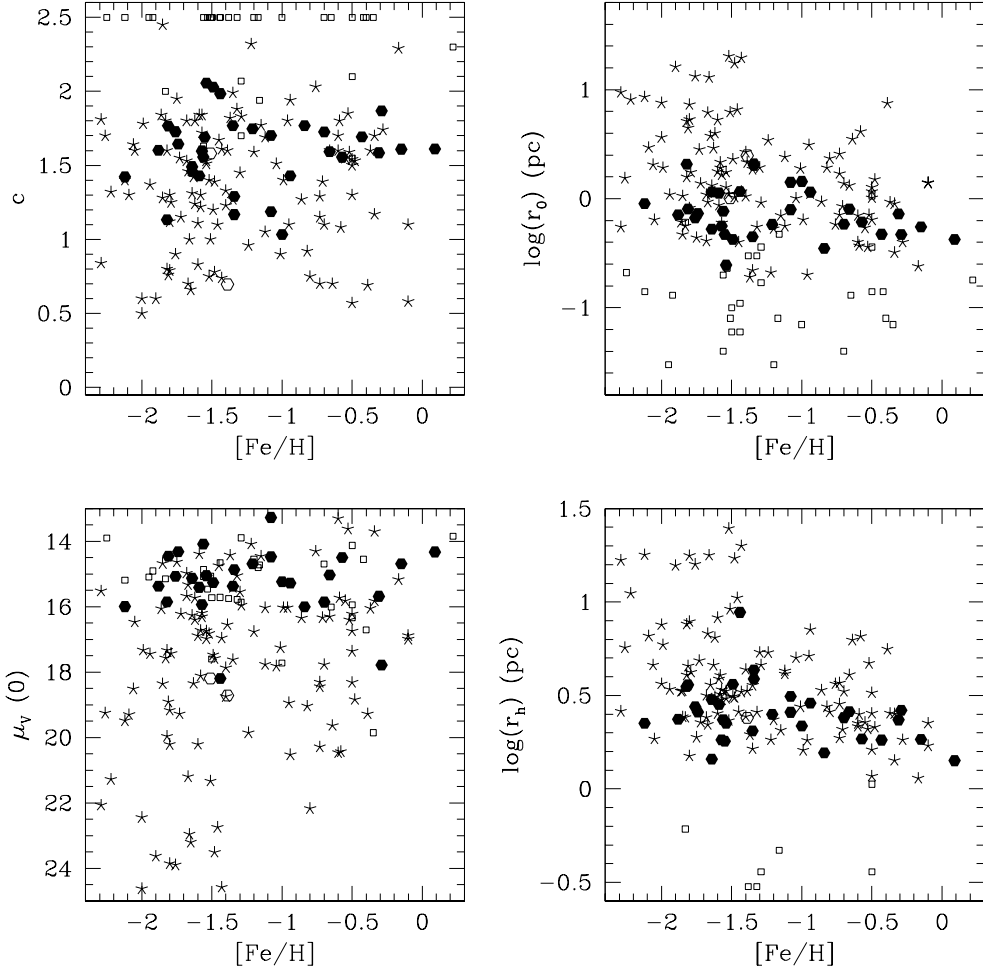


Fig. 9.— Metallicity versus structural parameters of M31 and Milky Way globular clusters. Symbols as in Figure 8.

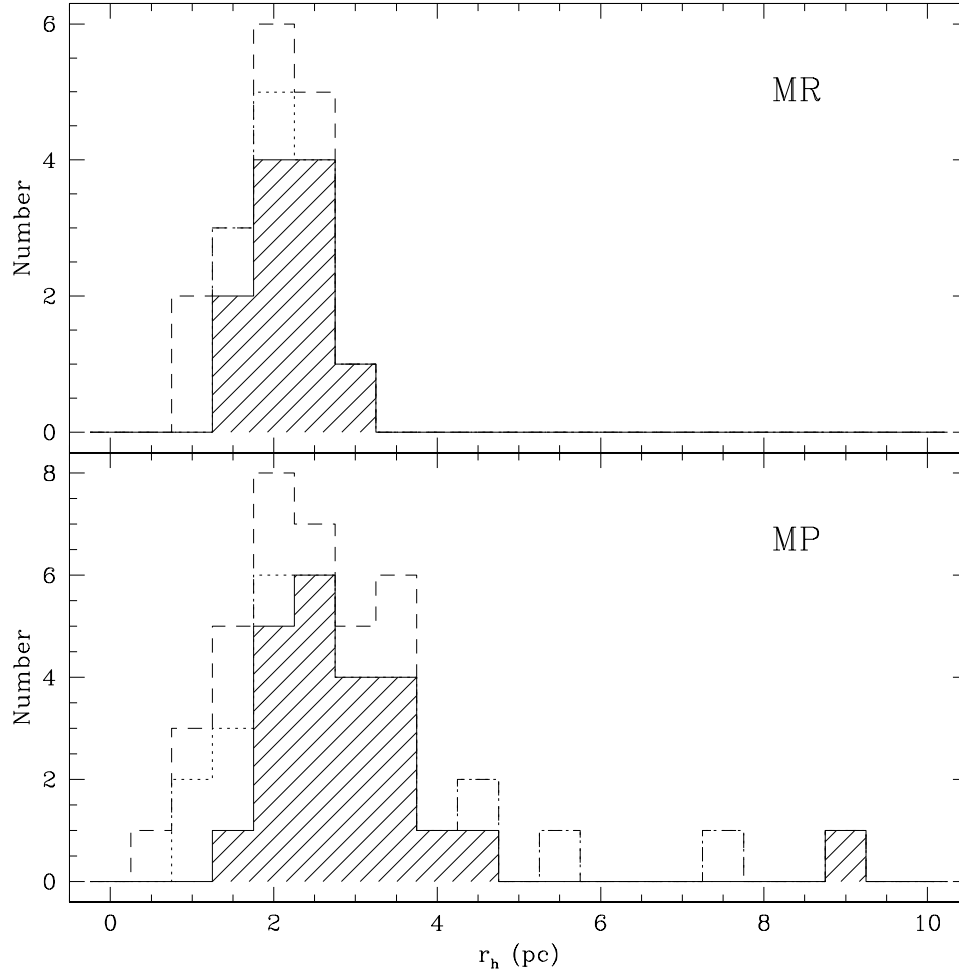


Fig. 10.— Size distribution of M31 globular clusters in two metallicity groups. Solid line/shaded histogram includes only clusters with spectroscopic metallicities. Dotted line histogram also includes clusters with color-derived metallicities from Barmby et al. (2000). Dashed line histogram also includes clusters with rough metallicity indicators from single colors.

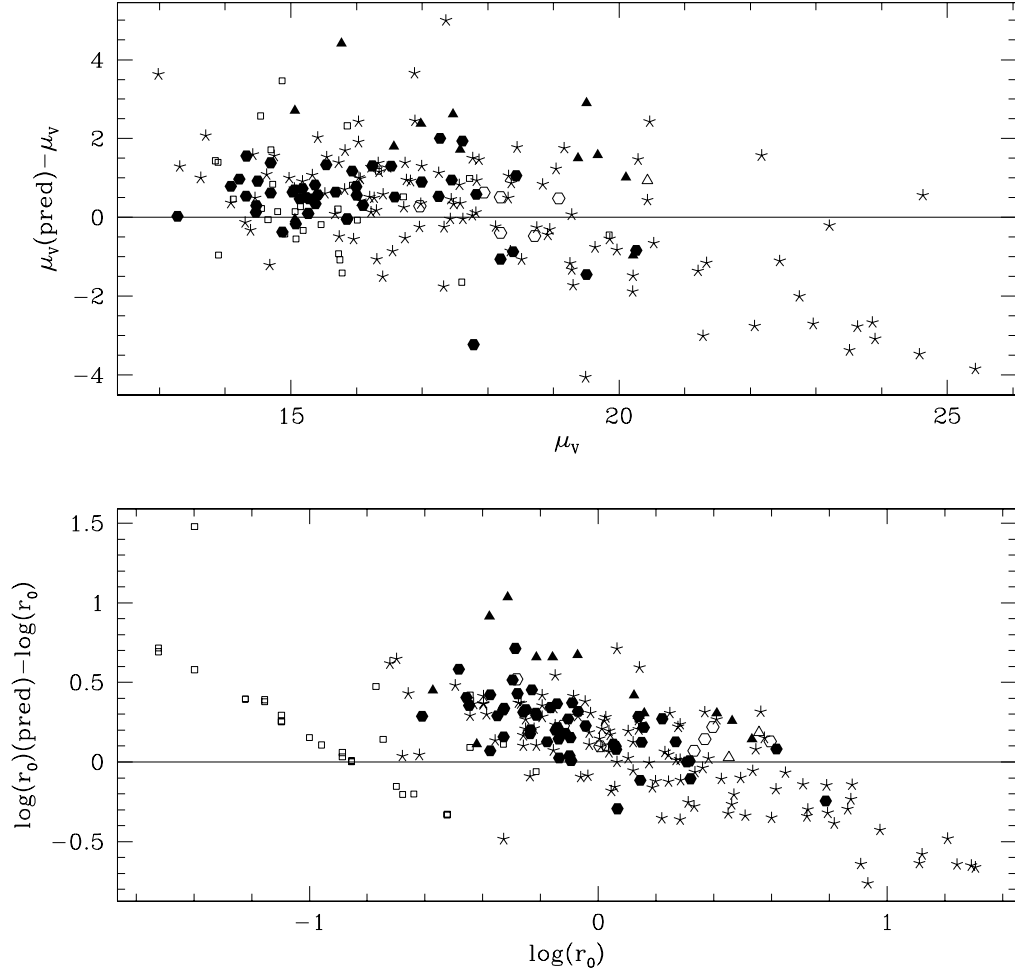


Fig. 11.— Difference between predicted (from the fundamental plane relations in McLaughlin 2000) and measured r_0 and $\mu_V(0)$ for M31 and MW GCs. The Milky Way constant mass-to-light ratio $\Upsilon_0 = 1.45$ was used to compute the predicted values. The apparent trend for the Milky Way core-collapsed clusters (small squares) is not meaningful since these objects do not have a core radius. Symbols as in Figure 8.

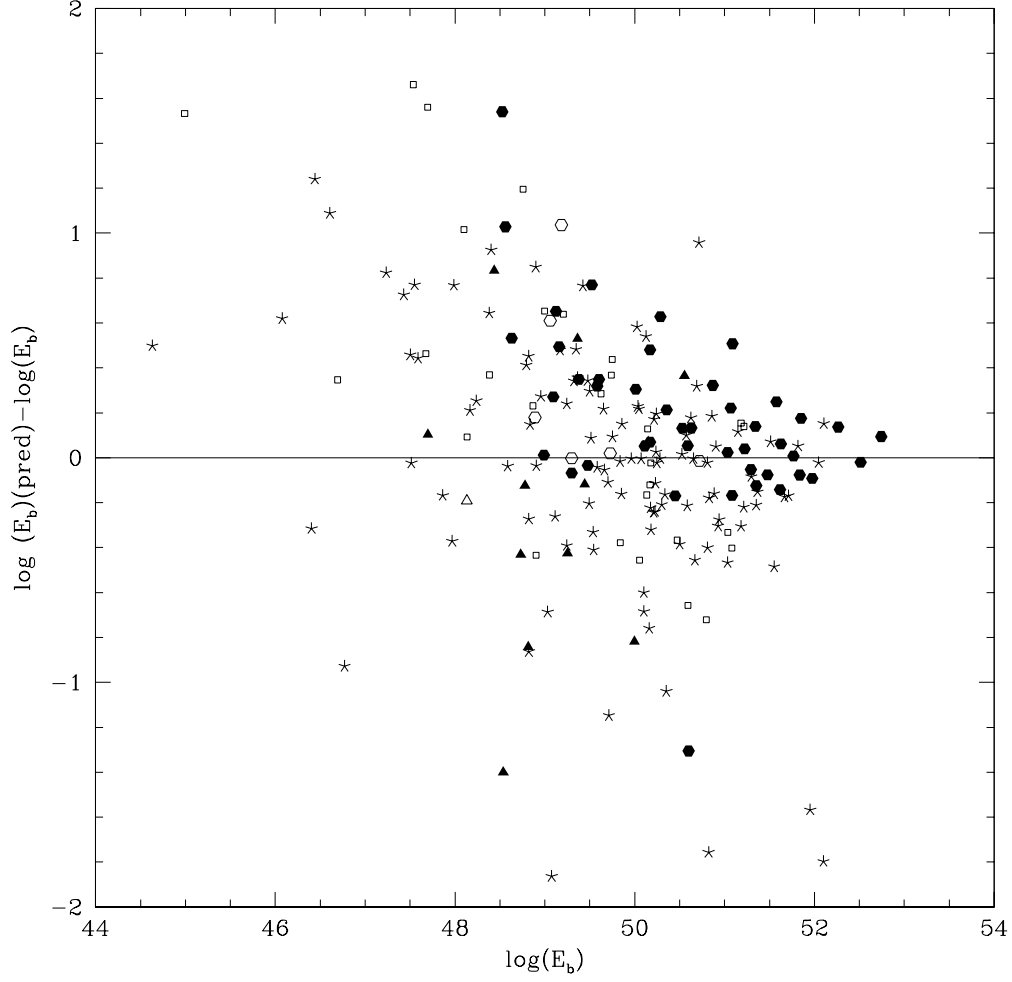


Fig. 12.— Difference between predicted (from the fundamental plane relations in McLaughlin 2000) and measured E_b for M31 and MW GCs. Symbols as in Figure 8.

Table 1. Shape parameters for GCs in M31 HST fields

name	ellipticity ^a	PA ^b	$r_0(\prime\prime)$ ^c	$r_t(\prime\prime)$	c	$\mu_V(0)$ ^d
000–001	0.20 ± 0.01	121 ± 1	0.21	10.50	1.70	13.65
000–D38	0.34 ± 0.04	108 ± 1	0.77	3.11	0.61	19.72
000–M091	0	0	1.09	4.42	0.61	20.56
006–058	0.08 ± 0.02	74 ± 2	0.16	5.76	1.56	15.00
009–061	0.12	31	0.15	5.86	1.60	15.23 (<i>I</i>)
011–063	0.09 ± 0.02	76 ± 6	$c0.06$	7.28	2.06	15.40
012–064	0.08 ± 0.01	46 ± 9	0.21	12.33	1.77	14.91
018–071	0.15 ± 0.04	4 ± 2	0.37	17.42	1.68	18.73
020D–089	0.14	21	0.16	6.36	1.60	16.18 (<i>I</i>)
027–087	0.07 ± 0.02	97 ± 29	0.30	8.72	1.46	16.63
030–091	0.10 ± 0.01	118 ± 17	0.21	5.50	1.42	17.32
045–108	0.08 ± 0.01	40 ± 1	0.30	8.14	1.43	15.94
058–119	0.10 ± 0.00	138 ± 1	0.20	7.29	1.56	14.56
064–125	0.06	53	$c0.12$	6.03	1.69	17.36 (F300W)
068–130	0.22 ± 0.02	42 ± 1	0.12	9.04	1.87	19.28
070–133	0	0	(edge)
076–138	0.09 ± 0.01	69 ± 1	0.12	6.92	1.77	16.12
077–139	0.14 ± 0.02	132 ± 10	(edge)
092–152	0.08	109	$c0.14$	4.28	1.49	18.07 (F300W)
097D–000	0	0	0.75	6.83	0.97	18.91 (<i>I</i>)
101–164	0.07	80	0.19	4.39	1.37	17.97 (F300W)
109–170	0.10 ± 0.03	72 ± 9	0.19	7.44	1.59	16.03
110–172	0.05	49	0.38	4.09	1.03	15.83
114–175	0.06 ± 0.01	132 ± 4	0.21	3.99	1.27	16.84
115–177	0.08 ± 0.02	63 ± 7	0.14	5.92	1.61	15.04
123–182	0.14 ± 0.04	62 ± 6	$c0.09$	6.34	1.83	16.93
124–NB10	0.07 ± 0.01	164 ± 3	0.22	3.89	1.25	14.56
127–185	0.08 ± 0.01	64 ± 4	0.37	5.74	1.19	15.04
128–187	0.08 ± 0.02	176 ± 1	0.13	3.49	1.36	15.25 (<i>I</i>)
132–000	0.09 ± 0.02	40 ± 59	0.16	1.59	1.00	15.63 (<i>I</i>)
134–190	0.16 ± 0.00	113 ± 1	(edge)
143–198	0.05 ± 0.01	158 ± 7	0.11	4.53	1.61	14.83
145–000	0.14	92	$c0.14$	3.36	1.39	19.43 (F300W)

Table 1—Continued

name	ellipticity ^a	PA ^b	$r_0(\prime\prime)^c$	$r_t(\prime\prime)$	c	$\mu_V(0)^d$
146–000	0.06	151	0.12	6.12	1.69	18.19 (F300W)
148–200	0.07	27	(edge)
153–000	0.05	70	(edge)
155–210	0.12 ± 0.01	80 ± 15	0.09	3.49	1.59	17.49
156–211	0.05 ± 0.02	67 ± 4	0.19	14.37	1.84	16.45
160–214	0.18 ± 0.00	2 ± 1	0.18	5.44	1.48	17.80
167–000	0.04	97	(edge)
205–256	0.08 ± 0.04	152 ± 22	0.53	9.12	1.17	17.14 (F300W)
231–285	0.17 ± 0.02	136 ± 33	c0.15	3.96	1.38	16.88
232–286	0.18 ± 0.01	42 ± 1	0.19	7.56	1.60	15.69
233–287	0.11 ± 0.02	74 ± 8	0.30	7.99	1.43	15.88
234–290	0.07 ± 0.01	71 ± 16	0.09	5.33	1.77	16.35
240–302	0.16 ± 0.01	98 ± 1	0.18	9.35	1.73	15.42
264–NB10	0.26 ± 0.04	142 ± 17	0.35	2.54	0.85	17.93
268–000	0.12 ± 0.04	103 ± 50	c0.14	1.56	1.06	17.62
279–D68	0.20 ± 0.09	79 ± 77	0.36	4.39	1.07	18.78
311–033	0.09 ± 0.01	54 ± 7	0.19	8.46	1.64	15.13
315–038	0.13 ± 0.02	159 ± 11	0.57	6.56	1.03	17.31
317–041	0.11 ± 0.02	66 ± 23	0.24	6.31	1.42	16.50
318–042	0.19 ± 0.03	70 ± 5	(edge)
319–044	0	0	0.62	4.73	0.88	18.54
324–051	0	0	0.66	3.19	0.69	19.06
328–054	0.27 ± 0.05	159 ± 5	0.27	10.70	1.58	18.54
330–056	0.14 ± 0.01	102 ± 8	0.44	3.62	0.91	18.17
331–057	0.24 ± 0.06	70 ± 3	0.31	29.53	1.98	18.54
333–000	0.23 ± 0.02	26 ± 17	0.49	5.83	1.08	19.85
338–076	0.06 ± 0.01	102 ± 34	0.55	10.74	1.29	15.34
343–105	0.09 ± 0.01	70 ± 22	c0.11	11.91	2.03	15.58
358–219	0.12 ± 0.02	63 ± 5	0.55	7.40	1.13	16.18
368–293	0	0	1.04	3.86	0.57	19.43
374–306	0.21 ± 0.02	106 ± 1	0.20	7.90	1.60	18.29
379–312	0.09 ± 0.02	55 ± 3	0.15	8.16	1.73	16.27
384–319	0.20 ± 0.01	121 ± 1	0.21	8.27	1.59	15.50

Table 1—Continued

name	ellipticity ^a	PA ^b	r_0 ($''$) ^c	r_t ($''$)	c	$\mu_V(0)$ ^d
386–322	0.08 ± 0.01	140 ± 3	0.15	8.54	1.75	15.05
468–000	0	0	1.61	11.55	0.86	20.61
NB39	0.13 ± 0.04	28 ± 17	0.22	1.26	0.75	17.96
M31GC J004304+412028	0.09 ± 0.04	75 ± 3	0.18	1.65	0.95	17.82
M31GC J004251+411035	0.10 ± 0.01	116 ± 20	c0.07	5.45	1.88	16.61
M31GC J004258+405645	0.18	175	0.11	0.80	0.86	17.33
M31GC J004301+405418	0.15 ± 0.04	30 ± 14	0.13	0.50	0.59	18.04
M31GC J004312+405303	0.38 ± 0.01	44 ± 4	0.68	3.06	0.66	21.46
M31GC J004103+403458	0.38 ± 0.14	87 ± 8	(edge)
M31GC J004537+413644	0	0	0.90	4.39	0.69	21.04
M31GC J004030+404530	0.19	123	0.10	10.66	2.03	15.31
M31GC J004027+414225	0.32 ± 0.06	128 ± 4	0.95	3.70	0.59	20.78
M31GC J004051+404039	0	0	0.38	4.26	1.05	20.45

^aEllipticity is defined as $\epsilon = 1 - (b/a)$, where a and b are the lengths of the semi-major and semi-minor axes, respectively

^bPosition angle is measured in degrees east from north

^c‘c’ indicates core-collapse candidates.

^dBandpass names indicate central surface brightness measured in other than V .

Table 2. Structural parameters for cluster 000–001 (G1)

Source	r_0 ($''$)	r_h ($''$)	r_t ($''$)	c	$\mu_V(0)$ (mag arcsec ^{−2})
this work	0.21	0.82	10.5	1.70	13.65
Rich et al. (1996)	0.17	0.70	28.2	2.22	13.5
Meylan et al. (2001)	0.14	3.7	54	2.59	13.47

Table 3. Fundamental plane predictions – measurements

	$\Delta \log(r_0)$	$\Delta \mu_V(0)$	ΔE_b	N
Milky Way	0.03 ± 0.03^a	0.15 ± 0.15	-0.03 ± 0.05	110
M31	0.20 ± 0.03	0.45 ± 0.14	0.25 ± 0.09	45

^aValues are mean $\pm \sigma/\sqrt{n}$.